ACS APPLIED MATERIALS & INTERFACES

Research Article

www.acsami.org

Development of Nanopatterned Fluorine-Doped Tin Oxide Electrodes for Dye-Sensitized Solar Cells with Improved Light Trapping

Fengli Wang,*[,†] Navaneetha K. Subbaiyan,[‡] Qian Wang,[†,§] Caitlin Rochford,[†] Guowei Xu,[†] Rongtao Lu,[†] Alan Elliot,[†] Francis D'Souza,*[,‡] Rongqing Hui,[†,§] and Judy Wu*[,†]

[†]Department of Physics and Astronomy, 1251 Wescoe Hall Drive, Malott Hall, University of Kansas, Lawrence, Kansas 66045, United States

[‡]Department of Chemistry, University of North Texas, 1155 Union Circle, #305070, Denton, Texas 76203, United States

[§]Department of Electrical and Computer Science, University of Kansas, Lawrence, Kansas 66045, United States

ABSTRACT: Transparent conductors (TCs) are an important component of optoelectronic devices and nanoscale engineering of TCs is important for optimization of the device performance through improved light trapping. In this work, patterned periodic arrays of nanopillars and nanolines of pitch size of ~700 nm were created on fluorine-doped tin oxide (FTO) using nanoimprint lithography and reactive ion etching using environmentally friendly gases. The patterned FTO exhibits enhanced light trapping as compared to the unpatterned FTO, which agrees well with simulations based on Finite-Difference Time-Domain method for up to a distance of 4 μm. Dye sensitized solar cells (DSSCs) fabricated on the patterned FTO exhibited improved performance (fill factor and power conversion efficiency), which can be attributed to enhanced light absorption in the range 400−650 nm. Further, electrochemical impedance measurements revealed lower recombination resistance for the patterned FTO/TiO_2 electrode compared to the unpatterned FTO electrode/TiO_2 electrode as a result of better light capturing properties of patterned FTO. The direct fabrication of nanopatterns on TCs developed in the present study is expected to be a viable scheme for achieving improved performance in many other optoelectronic devices.

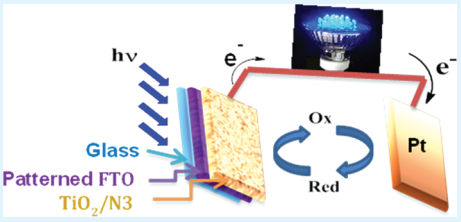

KEYWORDS: *photovoltaic, nanopatterned transparent conductors, light scattering, nanoimprint lithography, dye sensitized solar cells, fluorine-doped tin oxide*

1. INTRODUCTION

Transparent conductors (TCs) are essential components in optoelectronics such as solar cells, liquid crystal displays and light emitting diodes. Indium tin oxide (ITO) has been widely used in optoelectronics. However, the long-term use of ITO has severe limitations. Indium is scarce and consequently may become prohibitively expensive as the demand for PV devices increases.[1] Compared to ITO, fluorine doped tin oxide (FTO) is low cost, indium free, stable at high temperatures, and in acidic and hydrogen environments. Consequently, FTO has been widely used for devices that require high fabrication temperature and hydrogen containing environments such as organic light emitting diodes, organic solar cells, inorganic thin-film photovoltaics, and dye-sensitized solar cells (DSSCs). Improving light transmittance and scattering through nano-engineering of FTO may provide a direct scheme to enhance light absorption,[2] interfacial surface area,[3] and hence power conversion efficiency of solar cells that use FTO TC electrodes. Light scattering simulations have suggested that a periodic nanostructure between the absorber layer and a Bragg reflector may significantly increase light absorption below and near the band edge, up to an increase of 10-fold or higher.[2] Extensive studies have been made in integrating nanostructures into the photoactive layer[2,4,5] and back reflector[6] of solar cells. For example, periodic nanostructures embossed in the photoactive layer in organic solar cells demonstrated 3-fold absorption enhancements near the band edge of TDPTD:PCBM, resulting in efficiency improvement up to ~70%.[7]

Generation of nanostructures on transparent front electrodes may provide a unique advantage since the light trapping can be obtained directly on the photoactive layer without complications of additional interfaces. On FTO, nanostructures may be achieved via template growth. A recent work on growth of TiO_2-coated 3D inverse opal FTO nanostructures of 500 nm pitch size on commercial FTO substrates using solution-based process with self-assembled templates revealed strong light trapping.[8] Enhanced power conversion efficiency is expected in solar cells using this nanopatterned FTO as the cathode. It should be realized that solution-based lithography process suffers from lack of control in the geometry of the patterns generated.[9] Direct patterning of FTO using photolithography or nanoimprint lithography (NIL) may provide a straightforward scheme for enhancing light trapping and the geometry of the patterns can be readily controlled using photo masks or

Received: December 12, 2011
Accepted: February 10, 2012
Published: February 10, 2012

NIL stamps. A recent attempt to enhance the power conversion efficiency of DSSCs on patterned FTO using photolithography showed encouraging results, however, with large pitch sizes of 6−200 μm.[10] Reducing the feature dimension to subμm range is desired for trapping light in the visible spectrum. An additional difficulty in direct FTO patterning is in etching of FTO. Halogen gas (Chlorine) in inductively coupled plasma (ICP) has been employed to etch FTO[10,11] and was found degrading the FTO films.[10] To avoid the disadvantage of halogen gas in degrading FTO films and damaging the plasma apparatus, researchers adopted organic gas and electron cyclotron resonance (ECR).[12,13] Both ICP and ECR are relatively expansive techniques. Hence, development of lower cost etch processes using environmental friendly gases is necessary and important.

In this work, we have developed periodic subμm nanostructures on commercial FTO substrates using NIL and reactive ion etching (RIE). Both NIL and RIE processes are relatively low cost and scalable. In particular, alcohol vapor and hydrogen mixed gases were employed for FTO etching in RIE, which are environmental friendly and nondestructive to FTO film and RIE system. Two types of nanopatterns, nanopillars and nanolines, with pitches of 700 nm and heights up to 230 nm were generated on commercial FTO substrates. Theoretical simulations suggested enhanced light trapping in nanopatterned FTO at small TiO_2 thickness (up to 4 μm).[14] Consequently, DSSCs of TiO_2 thicknesses of 4 μm were constructed on these patterned FTO electrodes. The smaller thickness was particularly chosen to manifest the benefit of light trapping on patterned FTO. In agreement with the computational simulations, improved power conversion efficiency has been obtained for devices built on patterned electrodes as compared to the devices fabricated on the unpatterned FTO. These results are described in the following sections.

2. EXPERIMENTAL METHODS

2.1. Fabrication of Nanopatterned FTO. Figure 1 shows the schematic fabrication procedure of nanopatterned FTO. Commercial FTO glass TEC 8 (Hartford Glass Co. Inc.) was used for all the experiments. The thickness of FTO layer is approximately 550−600 nm on 3 mm thick glass. The FTO/glass was cleaned in an ultrasonic bath with detergent, DI water, acetone, and isopropanol in sequence. Polymer MRI-7030r (Micro Resist Technology GmbH) was spin coated onto cleaned FTO. NIL was performed on the polymer at 20−40 bar at 140 °C for 4 min with two types of stamps: nanopillar stamp (SNS-C14.3-0808-350-D45-P, Lightsmyth Technologies) and nanoline stamp (S2D-18C3−0808−350-P, Lightsmyth Technologies). Nanopillar stamp has 700 nm period, hexagonal pillar arrangement and 290 nm pillar diameter. Linear Si stamp has 700 nm period and 330 nm feature width. To avoid the direct surface contact between stamps and FTO, a thin layer of polymer was left in the grooves after nanoimprinting. The residual polymer layer was removed by O_2 plasma in the reactive ion etching (RIE) system. RIE of FTO was carried out using ethyl alcohol vapor and hydrogen gas. The plasma was generated at a pressure of 8 mTorr with a RF power of 300 W. The gas pressure ratio of hydrogen to alcohol was around 5:2. After etching, patterned FTO was cleaned using diluted HCl and DI water to remove possibly residues of the RIE process. Polymer mask was then removed using O_2 plasma.

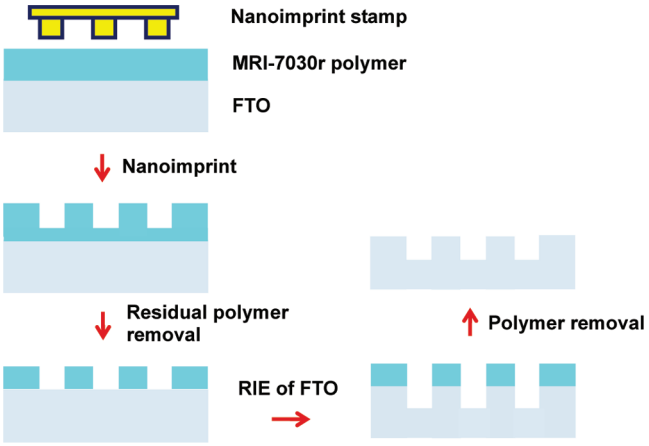

Figure 1. Schematic illustration of FTO patterning procedure using NIL and RIE.

2.2. Solar Cell Assembly Using Patterned FTO and Unpatterned FTO Electrodes. Patterned and unpatterned FTO electrodes for solar cell characterization were prepared under identical conditions to ensure good comparison. FTO glass plates were cleaned using the detergent by gently rubbing over the microcloth pads (BAS). After washing off the soap with DI water, they were further cleaned using 0.1 M HCl in ethanol, acetone, and isoproapanol solutions in an ultrasonic bath for 15 min sequentially. The electrodes were then heated at 450 °C to remove all the organic impurities. Then, a layer of TiO_2 (18NRT) paste was coated on the FTO glass plates using Doctor Blade technique. After leaving electrodes for 10 min to reduce the surface irregularity, they were heated gradually from 120 to 550 °C. After annealing, the TiO_2 films were treated with 40 mM $TiCl_4$ solution at 70 °C for 30 min and rinsed with water and ethanol, followed by annealing at 520 °C. Once TiO_2 layers were cooled to 80 °C, they were immersed in 0.2 mM N3 dye (DyeSol) in a mixture of acetonitrile and tert-butyl alcohol (1:1 volume) and kept at room temperature for 24 h. The thickness of the TiO_2 layer measured using a profilometer was found to be 4 μm. The counter electrode was prepared by depositing the Pt catalyst on the FTO glass (Tec 8, Pilkington) using a drop of H_2PtCl_6 solution (5 mg Pt in 1 mL ethanol) and heating at 40 °C for 15 min. The two electrodes were assembled and held together using 25 μm thick thermal sealant (Surlyn DyeSol). The electrolyte was filled using capillary effect. The electrolyte consist of 0.6 M propyl methyl imidazonium iodide (PMII), 0.1 M LiI, 0.05 M I_2 and 0.6 M 4-tert-butylpyride (TBP) in acetonitrile. The area of the electrode was controlled using a mask of 0.15 cm^2 area (5 mm × 3 mm).

2.3. Characterization. The transmittance and reflectance measurements were made using a iHR550 Imaging Spectrometer (Horiba) with Xe arc lamp light source. Reflectance and diffuse transmittance were measured by incorporating an integrating sphere (Labsphere) between the spectrometer's output and a calibrated silicon photodiode. The sample was situated at the entrance port of the sphere for transmittance measurements and at the port opposite the entrance port for reflectance measurements. During specular transmittance measurements, the sample was placed in the white light beam path before the input of the spectrometer, with the spectral output going directly to the silicon detector. The etching depth of FTO was measured with KLA Tencor P-16 profiler. Photovoltaic measurements of solar cells were performed using Model 2400 Current/Voltage Source Meter of Keithley Instruments, Inc. (Cleveland, OH) under illumination with an AM 1.5 simulated light source using a Model 9600 of 150 W Solar Simulator of Newport Corp. (Irvine, CA). Photoelectrode as negative (black) platinum foil as positive (red) results in negative anodic current and positive cathodic current. A 340 nm filter was introduced in the light path to eliminate UV radiation. The light intensity was monitored by using an Optical Model 1916-C Power Meter (Newport). Incident photon-to-current efficiency (IPCE) measurements were performed under ~2.5 mW cm^2 monochromatic light illumination conditions using a setup comprised of a 150 W Xe lamp with a Cornerstone 260 monochromator (Newport Corp., Irvine, CA).

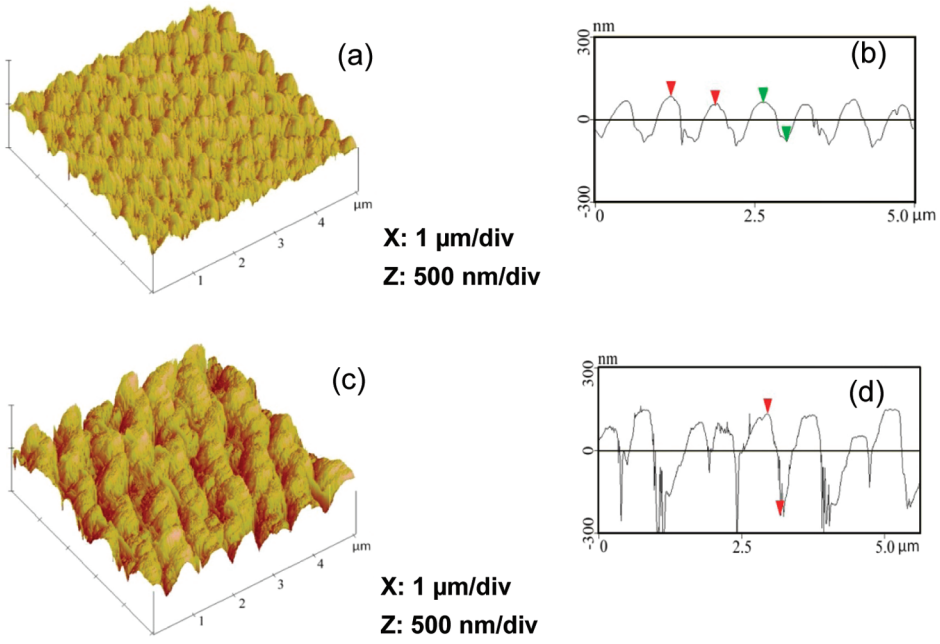

Figure 2. AFM images and section profiles of nanopatterned FTO (a, b) nano pillars and (c, d) nano lines. (a, c) 3D AFM images, (b, d) section analysis results. Scan area is 5 μm × 5 μm.

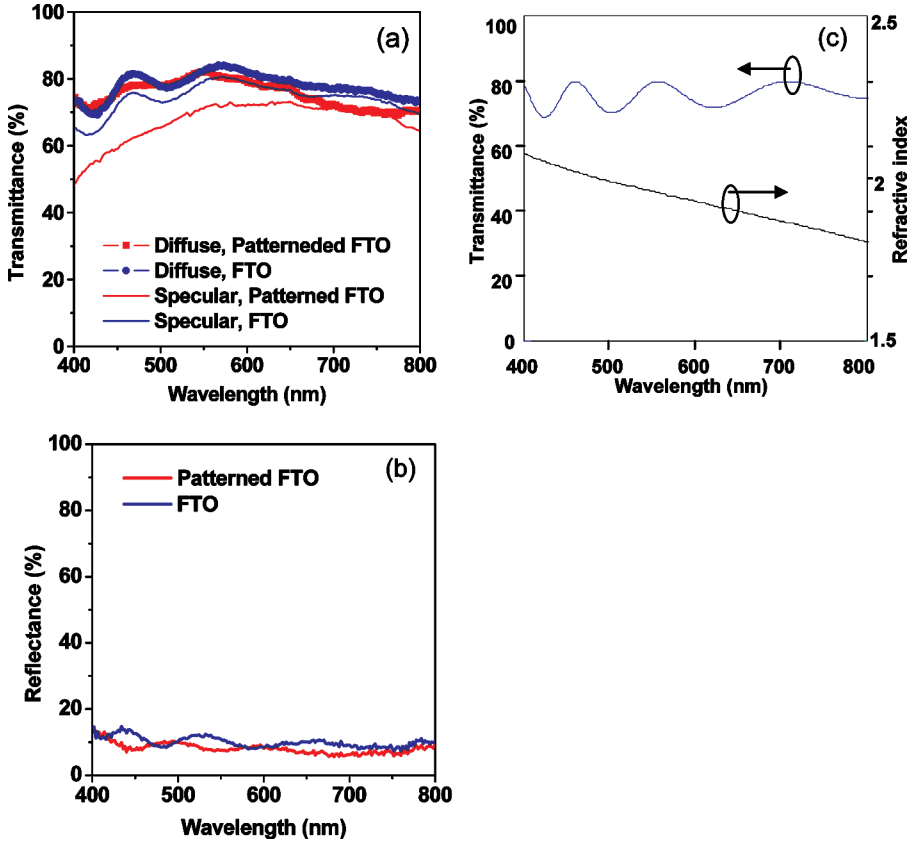

Figure 3. (a) Specular and diffuse transmittance of patterned FTO and unpatterned FTO, (b) reflectance of patterned FTO and unpatterned FTO surfaces on glass, (c) refractive index of FTO and calculated light transmittance as function of the wavelength.

3. RESULTS AND DISCUSSION

3.1. Morphology of the Patterned FTO. Atomic force microscopy (AFM) images and section analyses of FTO PC nanopillars and nanolines, respectively, are shown in Figure 2. The nanopillars [Figures 2(a) & (b)] have a pitch of about 665 nm, which is consistent with the specified pitch of 700 nm of the original Si grating. In the case of the FTO nanolines [Figures 2(c) & (d)], the lines do not appear straight and the gap width between the lines is not uniform. It should be noted that the nanostructures on FTO substrates have rough surface

dx.doi.org/10.1021/am201760q | ACS Appl. Mater. Interfaces 2012, 4, 1565–1572

morphology, which may be attributed to the original rough surface morphology of the commercial FTO, which was transferred through the patterning process employed in this experiment.

FTO is stable in hydrogen environment which led to etching difficulty and a low etching selectivity. Low etching selectivity can be inferred from the tapered nanopillars and ridged nanolines in images a and c in Figure 2 as follows. To etch FTO efficiently, we required a high power of 300 W. This caused a low etching selectivity, leading to the edges of the polymer mask eroding under high energy ion bombardment. Earlier, Kim et al. observed a rough surface for linear patterned FTO although they used TiO_2 as mask and $Cl_2-CH_4-H_2-Ar$ gas in plasma.[11] In fact, the rough surface is advantageous to the light scattering. It was reported that the light scattering was increased because of the tapered patterns.[15] Because nanopillars and nanolines have similar performance in terms of light scattering, the rest of the paper will focus on the nanolinear pattern with ~230 nm etching depth unless otherwise indicated.

3.2. Optical Properties of the Patterned FTO. Efficient light trapping offers solutions to improvement of light absorption and hence power conversion efficiency. Periodic structures of pitch size comparable to the wavelength of the incident light may provide efficient lights scattering, which increases the optical path length of light through diffracting incident light into highly oblique angles propagating in the adjacent active layer. Therefore, photon momentum can be scattered away from the specular direction by the designed periodic structure. To investigate the light scattering properties of the nanoline arrays compared to unpatterned FTO, we measured the specular and diffuse transmittance and total reflectance spectra; they are shown in panels a and b in Figure 3, respectively. In this measurement, a 570 nm thick FTO sample was attached to a thick glass. Specular transmittance refers only to light transmitted parallel to the incident light beam while diffuse transmittance includes all of the forward light (parallel and scattered) as measured with an integrating sphere. Light scattering is inferred from the difference between the diffuse and specular transmittance. Figure 3a indicates that the percentage of light scattered through the patterned FTO is inversely related to the wavelength with a value of ~10–25% in the 400–650 nm range with minimal scattering at wavelengths longer than 700 nm. In contrast, scattering from unpatterned FTO is roughly constant at ~10% in the entire visible wavelength range of 400–800 nm. Therefore, patterned FTO displays approximately 0–15% enhancement in scattering in the 400–650 nm range. The scattering occurring in the 400–650 nm range is primarily due to optical scattering on the corrugated FTO surface. The ridged linear array displays a maximum pitch of ~700 nm at the mouth of the grooves and has a narrow bottom (Figure 2c, d). Photons with wavelength less than ~700 nm will be scattered by the periodic grooves. Figure 3b reveals that patterned FTO reflects ~0–5% less light than unpatterned FTO in the range of 400–800 nm. The refractive index of FTO decreases slightly when the wavelength increases from 400 to 800 nm as shown in Figure 3c.[16] For the 570 nm thick FTO sample without surface patterning, a weak Fabry–Perot cavity exists between the two surfaces of the film. Therefore the power transmittance can be calculated with

$$T(\lambda) = \frac{\eta(1-R)^2}{(1-\eta R)^2 + 4\eta R \sin^2(2\pi nd/\lambda)} \quad (1)$$

where $R = [(n-1)/(n+1)][(n-1.5)/(n+1.5)]$ is the combined reflectivity of the two facets considering one of the two facets is on a thick glass with the index of 1.5. The symbol d represents the thickness of the FTO, and η is the power attenuation through the film. Figure 3c also shows the calculated power transmittance across the FTO film with η = 0.8 and d = 570 nm, which indicates characteristic Fabry–Perot resonance similar to that shown in Figure 3a. With nanostructure patterning on surface of FTO film, the Fresnel reflectivity is significantly reduced ($R \approx 0$) because of the strong scattering, and the Fabry–Perot resonance is thus eliminated from the transmittance spectra as indicated in Figure 3a. In general, for wavelengths much longer than the feature size, Rayleigh scattering dominates, in which the scattering efficiency is inversely proportional to the fourth power of the wavelength. On the other hand, if the size of the surface structure is on the same order of the wavelength, the scattering is in the Mie regime, and the specular transmittance becomes oscillatory as the function of the wavelength due to the coherent resonance of light in the structure.[17] Figure 3c shows a significantly reduced transmittance in the short wavelength region due to strong scattering. This will be further discussed in a later section and compared with numerical simulations.

3.3. Resistance of Etched FTO. If this nanostructured FTO is to be used as an electrode in a solar cell, it is not sufficient to only improve the light scattering into the device but the conductivity must remain high so that the optical benefit may translate into improved device performance and not be canceled by a competing deleterious effect. To compromise the transmittance and conductivity, we needed to select a proper etching depth. To determine the maximum etch depth at which the conductivity reduction remains mild, we etched a series of unpatterned FTO electrodes with various thickness using RIE. The resistance was measured with a digital multimeter. With respect to resistance, there is a well-known relationship for regular three-dimensional conductor, $R = \rho L/W(t-d)$, where R is resistance, ρ is resistivity, L is the length, W is width, t is the original FTO sheet thickness, and d is the etch depth. The results are summarized in the $\log(R/R_0)$ vs d curve in Figure 4, where R_0 is the resistance of the FTO before etching. Two approximately linear trends of dramatically different slopes can be clearly seen with the lower slope one in the low d range below 230 nm and the higher one in the higher d range. The former is expected from the reduction of the total conducting sheet thickness while the latter may be caused by disconnection of remaining FTO islands, which form

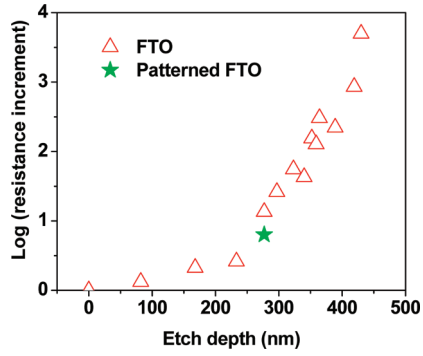

Figure 4. Resistance increment as a function of etching depth in FTO layer.

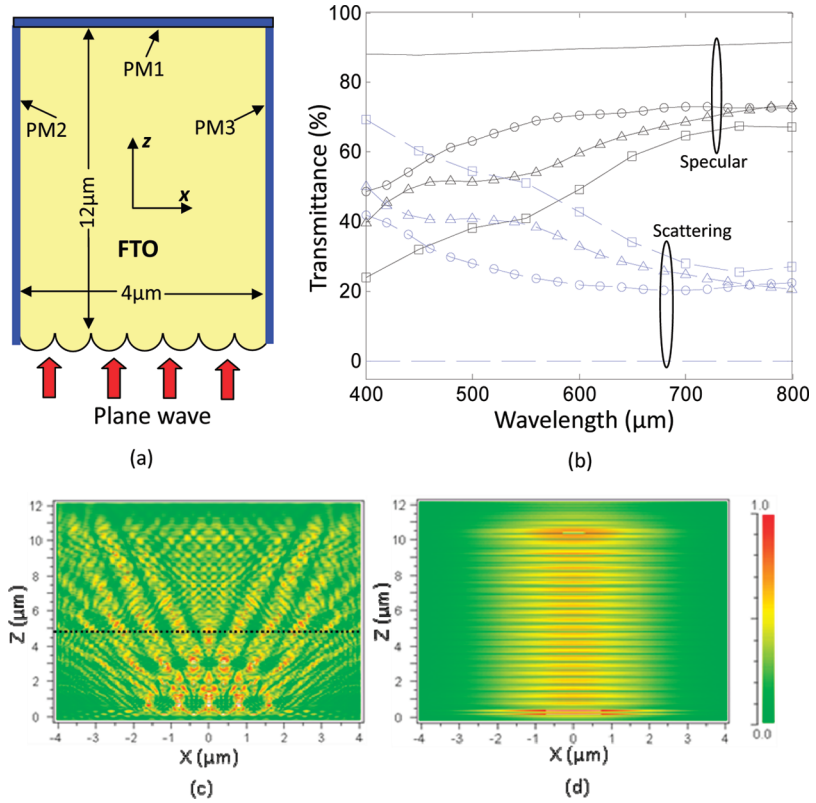

Figure 5. (a) Geometric configuration of simulation where PM1, PM2 and PM3 are power monitor. (b) Calculated specular transmittance (solid lines) and scattering (dashed lines) for the FTO surface without rigid structures (no symbols), with 350 nm (circles), 500 nm (triangles) and 800 nm (squares) hemispheres. (c) Power distribution of a Gaussian beam passing across a patterned air/FTO interface, and (d) Power distribution of a Gaussian beam passing across a flat air/FTO interface.

when the etch depth is large enough to make FTO no longer a continuous sheet. In fact, R increased 2.6 fold from R_0 at $d \approx$ 230 nm, whereas R jumped by 13.5 fold at $d \approx$ 277 nm. Therefore, the threshold etching depth to maintain reasonable sheet conductance is around 230 nm. The resistance in patterned FTO exhibited a qualitatively similar trend while a lower resistance increment of approximately 6 fold was observed at $d \approx$ 277 nm, which is not surprising, because FTO is only partially removed in this case.

3.4. Simulation of Optical Behavior of Patterned FTO Surface. Numerical simulations using a Full-wave simulation package[24] based on finite-difference time-domain (FDTD) method was performed in order to calculate the light scattering in the patterned FTO. As illustrated in Figure 5a, in the simulation, a plane wave propagates upward toward the air/FTO interface. The width of the simulation area is ±2 μm and the grid size for FTDT simulation is 2 nm near the boundary and 20 nm elsewhere to trade-off the accuracy and simulation time. A power monitor PM1 is placed 12 μm away from the input to measure the specular transmitted power (P_1) in the z-direction across the interface. Other two power monitors PM2 and PM3 are placed on the sides of the simulation window to measure scattered optical power into ± x directions (P_2 and P_3). Figure 5b shows the optical power P_1 (solid lines) and P_2 + P_3 (dashed lines) obtained from the simulation. Without hemispherical structure on the FTO surface, only Fresnel reflection existed and the scattering is zero. The wavelength-dependency of the transmittance is weak only due to the wavelength-dependent refractive index of FTO as previously discussed in Figure 3c. With hemispheres on the FTO surface, significant scattering was introduced which decreases the power in the specular direction, whereas the scattered power in the ±x directions is increased. The results show that the effect of scattering is stronger in the short wavelengths near 400 nm. Although the absolute value of specular transmittance depends on the size of the power monitor PM1, the wavelength dependency of scattering shown in Figure 5b agrees with the measured results in Figure 3a. Three diameters of the hemispheres, 350, 500, and 800 nm, were used in the simulation; the results suggest that hemispheres with larger sizes would introduce stronger scattering.

Figure 5c shows an example of light-wave propagation into the FTO layer with 5 hemispheres on the input surface and the diameter of each hemisphere was 800 nm. In this simulation, a Gaussian beam with 4 μm width was launched upward through the patterned surface. Wave scattering and interference between fields scattered from different hemispheres are clearly seen. In the solar cell application, the propagation of scattered wave in the ±x directions increases the path length inside the absorption layer, and therefore helps the increase in conversion efficiency within this layer. It should be pointed out that the benefit of light scattering by the nanopatterns is primarily located near the interface of the nanopatterns. It may be noted here that at larger thickness, that is, distances beyond 4 μm, this effect becomes negligible. As a comparison, Figure 5d shows that without the patterned structure on the FTO surface, no scattering was introduced. Power monitors PW2 and PW3 placed on each side wall would not see any optical power propagating in the ±x directions.

dx.doi.org/10.1021/am201760q | ACS Appl. Mater. Interfaces 2012, 4, 1565−1572

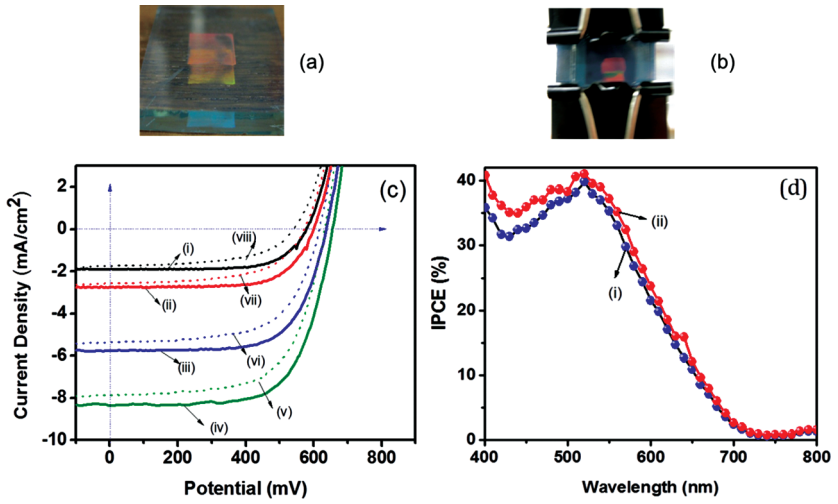

Figure 6. (a) Picture of patterned FTO electrode, (b) picture of photocell assembled using patterned electrode, (c) $J-V$ characteristics of the patterned (solid line i–iv) and unpatterned (dashed line v to viii) of FTO/TiO_2/N3 in the presence of I^-/I_3^- redox mediator in acetonitrile under different light power density for the 4 μm thick TiO_2 electrodes, and (d) Incident photon-to-current conversion efficiency (IPCE%) for patterned (ii) and unpatterned (i) FTO/TiO_2/N3 electrodes in the presence of I^-/I_3^- redox mediator in acetonitrile.

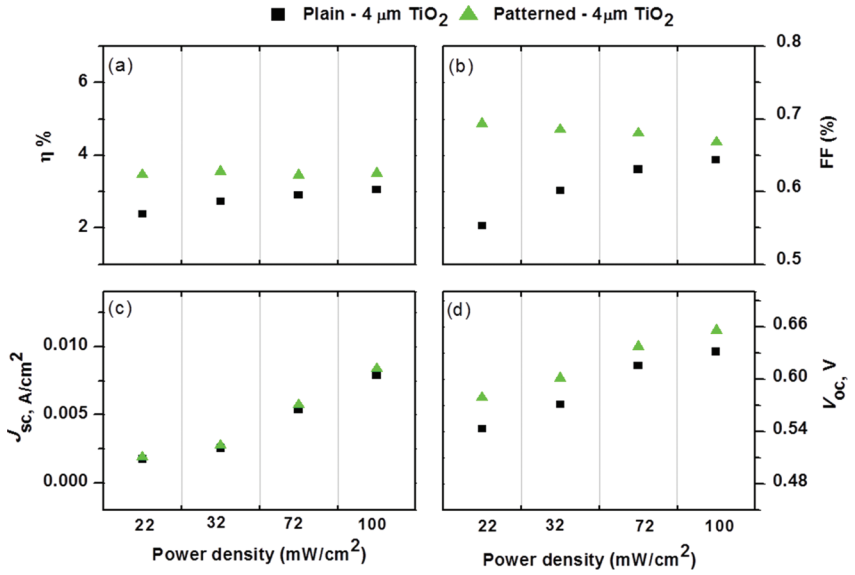

Figure 7. Figures of merit of the patterned versus unpatterned FTO electrodes: (a) overall light conversion efficiency, η%, (b) fill-factor, FF%, (c) short circuit current, J_{SC} and (d) open circuit potential, V_{OC} under different light power densities. Electrodes of 4 μm thick TiO_2 layer on patterned and unpatterned (plain) FTO were used, and recorded in acetonitrile containing 0.6 M PMII, 0.1 M LiI, 0.05 M I_2 and 0.5 M TBP as redox mediator.

3.5. Dye-Sensitized Solar Cell Performance. Motivated by the improved light scattering, reduced reflectance, acceptable added resistance, and theoretical predictions of better light trapping at lower thickness, DSSCs were fabricated on the patterned and unpatterned FTO in order to determine whether the solar cell performance could be improved. To align with the theoretical predictions, electrodes of TiO_2 film thickness of 4 μm were fabricated, which is much lower than the traditionally used ~10 μm thick TiO_2 film electrodes in literature. Details of the electrode fabrication and device assembly are given in the Experimental Section. The amount of N3 dye adsorbed onto the TiO_2 layer was found to be 8.4 ± 10^{-8} moles cm^{-2}. Figure 6a shows the optical image of a patterned FTO; holding the electrode at an angle resulted in light diffraction that could be easily seen with the naked eyes. After surface modification with TiO_2, annealing at 550 °C, N3 adsorption, and assembling of the DSSC using I^-/I_3^- electrolyte, the cell was viewed at an angle. As shown in Figure 6b, diffracted light could be easily seen from the patterned portion of the FTO on the DSSC. These results indicate that during DSSC fabrication the patterned photonic structure was still retained.

Figure 6c shows $J-V$ characteristics of the DSSC on patterned and unpatterned FTO under different light power for the 4 μm thick TiO_2 electrodes. As shown in Figure 6c, steady anodic photocurrents were observed for both electrodes when they were illuminated using different light intensities, and under the experimental conditions no desorption of either the TiO_2 or the dye from patterned electrode was observed. For the patterned electrode, there was an increase in both the short circuit current, J_{SC}, and the open circuit potential, V_{OC}, compared to the results on unpatterned electrode, irrespective of the light intensity. Further photoaction spectra for these

dx.doi.org/10.1021/am201760q | ACS Appl. Mater. Interfaces 2012, 4, 1565–1572

samples were measured as shown in Figure 6d. The incident photon-to-current conversion (IPCE%) efficiencies for the patterned electrodes were 2−5% higher in the 400−650 nm range, however, above 650 nm only marginal effect was observed. These results agree well with the scattering data in Figure 3 and simulation predictions in Figure 5 where more light scattering from the patterned FTO compared to unpatterned FTO in the wavelength range 400−650 nm is expected. Since the light scattering enhancement wavelength range is determined by the pitch dimension of the PC patterned on FTO, further design and engineering the geometry of the nanostructure and the pitch dimension may allow the benefit to be extended to broader wavelength range. Nevertheless, these observations reveal a light scattering effect from patterned FTO that improves the performance of solar cells in a large portion of the visible spectrum.

The performance of the DSSCs in terms of the overall power conversion efficiency (η), fill-factor (FF), J_{SC}, and V_{OC} is shown in Figure 7. The η values remained constant to about 3.5% regardless of the incident light power density for the patterned electrode while this value increased steadily from 2.38 to 3.07% for unpatterned electrodes by increasing the light power density from 22 to 100 mW cm^{-2} (Figure 7a). The overall low η values could be attributed to smaller thickness of TiO_2 layer.

Both J_{SC} and V_{OC} were found to be higher for patterned electrodes compared to the unpatterned electrodes and both values increased with increasing the light intensity as shown in panels c and d in Figure 7. This would result in a better FF for the patterned electrode at low light power as shown in Figure 7b, which decreased slowly with increasing the light power. As expected, a steady increase in FF upon increasing the light power was observed for the plain FTO/TiO_2 electrode.

We also recorded the impedance of the two electrodes in which the patterned FTO/TiO_2 electrode showed lower recombination resistance compared to unpatterned FTO/TiO_2 electrode even under low light intensity of 22 mW/cm^2, as shown in the Figure 8. This is mainly attributed to the better light capturing properties of patterned FTO due to photonic effect,[18,19] without attributing to any series resistance. In this regard, photonic crystal[20,21] sensitized DSSCs and TiO_2 nanotubes[22] with light scattering properties are known for enhanced performance.

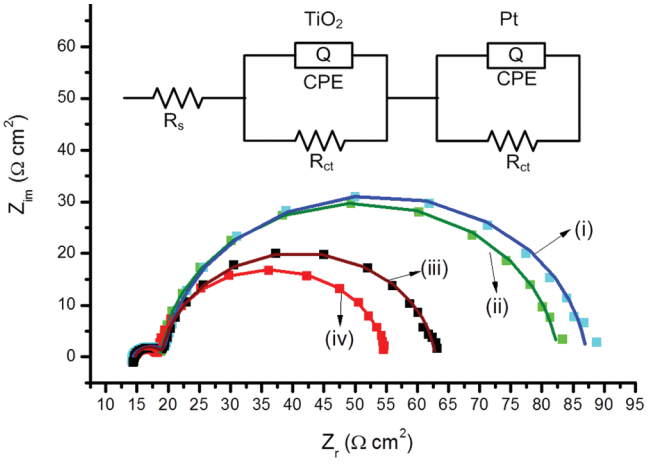

Figure 8. Impedance spectra (Nyquist plots) measured at the respective V_{oc} of patterned FTO/TiO_2 and plain FTO/TiO_2 in dark (i and ii) and under 0.22 sun at AM 1.5 light conditions (iii and iv), respectively. The figure inset shows equivalent circuit diagram used to fit the data.

4. CONCLUSIONS

Nanopatterned FTO was fabricated with nanoimprint lithography and RIE. Nanopillar and nanoline arrays were obtained on commercial FTO. While the resistance of the nanopatterned FTO increased with etching depth, a threshold of low resistance increment was found around 230 nm of etching depth. Enhanced light scattering was observed from nanopatterned FTO in the wavelength of 400−650 nm, which resulted in the improved power conversion efficiency of DSSCs fabricated atop. Simulation confirmed the deviation of the light propagation angled away from the surface normal onto the FTO nanostructure. When nanostructure corrugation is introduced on the FTO surface, phase distortion is created on the transmitted light beam, resulting in light scattering across the interface. As a result, an approximately 2−5% improvement of IPCE% efficiency was experimentally obtained on DSSCs with 4 μm TiO_2 layer in the wavelength range of 400−650 nm. Both J_{SC} and V_{OC} are found to be higher for patterned electrodes, resulting in enhanced power conversion efficiency as compared to the unpatterned electrodes. Since the nanopatterns are directly fabricated in TCs, this approach may provide a viable scheme for achieving high device performance in many optoelectronic devices.

AUTHOR INFORMATION

Corresponding Author

*E-mail: f205w094@ku.edu (F.W.); francis.dsouza@unt.edu (F.D.); jwu@ku.edu (J.W.).

Notes

The authors declare no competing financial interest.

ACKNOWLEDGMENTS

This work was supported in part by ARO (W911NF-09-1-0295), National Science Foundation (0803149, 1105986, 1110942, and EPS-0903806), and matching support from the State of Kansas through Kansas Technology Enterprise Corporation, a Grant-in-Aid (20108010 and 21750146). C.R. acknowledges a NSF Graduate Research Fellowship.

REFERENCES

(1) Kumar, A.; Zhou, C. *ACS Nano* **2010**, *4*, 11−14.
(2) Zhou, D.; Biswas, R. *J. Appl. Phys.* **2008**, *103*, 093102−5.
(3) Fan, Z.; Razavi, H.; Do, J.-W.; Moriwaki, A.; Ergen, O.; Chueh, Y.-L.; Leu, P. W.; Ho, J. C.; Takahashi, T.; Reichertz, L. A.; Neala, S.; Yu, K.; Wu, M.; Ager, J. W.; Javey, A. *Nat. Mater.* **2009**, *8*, 648−653.
(4) Tumbleson, J. R.; Ko, D.-H.; Samulski, E. T.; Lopez, R. *Appl. Phys. Lett.* **2009**, *94*, 043305−3.
(5) Gomard, G.; Drouard, E.; Letartre, X.; Meng, X.; Kaminski, A.; Fave, A.; Lemiti, M.; Garcia-Caurel, E.; Seassal, C. *J. Appl. Phys.* **2010**, *108*, 123102−8.
(6) Zeng, L.; Bermel, P.; Yi, Y.; Alamariu, B. A.; Broderick, A. K.; Liu, J.; Hong, C.; Duan, X.; Joannopoulos, J.; Kimerling, L. C. *Appl. Phys. Lett.* **2008**, *93*, 221105−3.
(7) Ko, D.-H.; Tumbleston, J. R.; Zhang, L.; Williams, S.; DeSimone, J. M.; Lopez, R.; Samulski, E. T. *Nano Lett.* **2009**, *9*, 2742−2746.
(8) Yang, Z.; Gao, S.; Li, W.; Vlasko-Vlasov, V.; Welp, U.; Kwok, W.-K.; Xu, T. *ACS Appl. Mater. Interfaces* **2011**, *3*, 1101−1108.
(9) Catchpole, K. R.; Mokkapati, S.; Beck, F.; Wang, Er.-C; McKinley, A.; Basch, A.; Lee, J. *MRS Bull.* **2011**, *36*, 461−467.
(10) Kong, S. M.; Xiao, Y.; Kim, K. H.; Lee, W. I.; Chung, C. W. *Thin Solid Films* **2011**, *519*, 3173−3176.

(11) Kim, S.-S.; Chun, C.; Hong J.-C. Kim, D.-Y. *J. Mater. Chem.* **2006**, *16*, 370−375.
(12) Minami, T.; Miyata, T.; Iwamoto, A.; Takata, S.; Nanto, H. *Jpn. J. Appl. Phys.* **1988**, *27*, L1753−L1756.
(13) Miyata, T.; Minami, T.; Sato, H.; Takata, S. *Jpn J. Appl. Phys.* **1992**, *31*, 932−937.
(14) Chen, J.-G.; Chen, C.-Y.; Wu, S.-J.; Li, J.-Y.; Wu, C.-G.; Ho, K.-C. *Sol. Energy Mater. Sol. Cells* **2008**, *92*, 1723−1727.
(15) Byeon, K.-J.; Hong, E.-J.; Park, H.; Yang, K.-Y.; Baek, J. H.; Jhin, J.; Hong, C.-H.; Kim, H. G.; Lee, H. *Semicond. Sci. Technol.* **2009**, *24*, 105004−5.
(16) Rottkay, K. V.; Rubin, M. *Mater. Res. Soc. Symp. Proc.* **1996**, *426*, 449.
(17) Hulst, H. C. V. D. In *Light Scattering by Small Particles*; Dover Publications: New York, 1957.
(18) Subbaiyan, N. K.; Maligaspe, E.; D'Souza, F. *ACS Appl Mater Interfaces* **2011**, *3*, 2368.
(19) Wang, Q.; Moser, J.-E.; Grätzel, M. *J. Phys. Chem. B* **2005**, *109*, 14945.
(20) Colodrero, S.; Mihi, A.; Haggman, L.; Ocana, M.; Boschloo, G.; Hagfeldt, A.; Miguez, H. *Adv. Mater.* **2009**, *21*, 764.
(21) Mihi, A.; Zhang, C. J.; Braun, P. V. *Angew. Chem., Int. Ed.* **2011**, *50*, 5711.
(22) Yip, C. T.; Huang, H. T.; Zhou, L. M.; Xie, K. Y.; Wang, Y.; Feng, T. H.; Li, J. S.; Tam, W. Y. *Adv. Mater.* **2011**, *23*, 5624.
(23) Bessho, T.; Zakeeruddin, S. M.; Yeh, C.-Y.; Diau, E. W.-G.; Grätzel, M. *Angew. Chem., Int. Ed.* **2010**, *122*, 6796.
(24) *FullWAVE Simulation Package*; R-soft Inc.: Ossining, NY.